Journal of Computational Neuroscience 9, 271–291, 2000

Alpha-Frequency Rhythms Desynchronize over Long Cortical Distances: A Modeling Study

STEPHANIE R. JONES
Department of Mathematics and Center for BioDynamics, Boston University, 111 Cummington Street, Boston, MA 02215
stephr@math.bu.edu

DAVID J. PINTO
Department of Mathematics and Center for BioDynamics, Boston University, 111 Cummington Street, Boston, MA 02215; Department of Neuroscience, Brown University, Providence, RI 02912

TASSO J. KAPER AND NANCY KOPELL
Department of Mathematics and Center for BioDynamics, Boston University, 111 Cummington Street, Boston, MA 02215

Received ; Revised ; Accepted

Abstract. Neocortical networks of excitatory and inhibitory neurons can display alpha(α)-frequency rhythms when an animal is in a resting or unfocused state. Unlike some γ- and β-frequency rhythms, experimental observations in cats have shown that these α-frequency rhythms need not synchronize over long cortical distances. Here, we develop a network model of synaptically coupled excitatory and inhibitory cells to study this asynchrony. The cells of the local circuit are modeled on the neurons found in layer V of the neocortex where α-frequency rhythms are thought to originate. Cortical distance is represented by a pair of local circuits coupled with a delay in synaptic propagation. Mathematical analysis of this model reveals that the h and T currents present in layer V pyramidal (excitatory) cells not only produce and regulate the α-frequency rhythm but also lead to the occurrence of spatial asynchrony. In particular, these inward currents cause excitation and inhibition to have nonintuitive effects in the network, with excitation delaying and inhibition advancing the firing time of cells; these reversed effects create the asynchrony. Moreover, increased excitatory to excitatory connections can lead to further desynchronization. However, the local rhythms have the property that, in the absence of excitatory to excitatory connections, if the participating cells are brought close to synchrony (for example, by common input), they will remain close to synchrony for a substantial time.

Keywords: rhythms, synchrony, cortex, alpha, attention

1. Introduction

Populations of neocortical neurons in animals are known to exhibit rhythmic activity during certain behavior states. Synchrony between rhythms recorded in distant cortical areas is thought to reflect a functional correlation between the areas (Farmer, 1998; Fries et al., 1997; König et al., 1995; Roelfsema et al., 1997; von Stein et al., 1999). Experiments in the visual cortex have shown that synchronous activity within and between visual areas correlates with perception and is usually associated with oscillatory firing patterns in the γ-frequency range of 30 to 80 Hz (Fries et al., 1997; König et al., 1995). A recent study shows that when

an animal switches from focused to resting behaviors, rhythms recorded from distant cortical areas (visual and parietal, and/or parietal and motor) switch from exhibiting zero-time lag synchrony (at β frequencies of 20 to 25 Hz) to being asynchronous (Roelfsema et al., 1997). During the periods when asynchrony is recorded, power spectra show strong bands of α-frequency (8 to 12 Hz) rhythms. In another study, coherence in the α and θ (6 to 8 Hz) frequency regimes were associated with significant phase lags (von Stein et al., 1998).

Analysis has shown that the structures of networks generating γ- and β-frequency rhythms are good for promoting synchrony (Ermentrout and Kopell, 1998; Karbowski and Kopell, 2000; Kopell et al., 2000). In this study, we investigate how the structure of α-frequency rhythms may facilitate asynchrony over distances. To understand the inability of α-frequency rhythms to synchronize over distances, we propose a model of a neocortical network that oscillates in the α-frequency range. Using the model, we show how intrinsic cellular and network mechanisms result in a lack of synchrony over distances. In some of the parameter regimes investigated, the model uses nonlinear interaction that depends on the inhibitory cell firing two spikes per cycle, known as doublets (Traub et al., 1996, 1999). These interactions produced synchrony in the cases of γ and β (Ermentrout and Kopell, 1998; Kopell et al., 2000) but asynchrony in the current case.

Our model (see Section 2, Methods) consists of synaptically coupled excitatory and inhibitory cells, and it is based on physiological data from layer V of the cortex, where α-frequency rhythms are thought to originate (Connors and Amitai, 1997; da Silva, 1991; Flint and Connors, 1996; Kristiansen and Courtois, 1949; Silva et al., 1991). A central feature of many of the pyramidal (excitatory) cells in layer V is the presence of two inward currents, known as h and T currents, whose time courses are consistent with α-frequency rhythms (Castro-Alamancos and Connors, 1996a, 1996b). Experiments have shown that pyramidal cells containing these currents produce augmented EPSPs in response to inhibitory stimulation that is synaptically generated at 10 Hz (α-frequency); however, faster stimulation (20 Hz) does not produce augmented responses. Furthermore, *in vivo* augmented responses are observed in layer V cells during periods of rest or immobility (Castro-Alamancos and Connors, 1996a, 1996b; Huguenard and McCormick, 1992), precisely when α-frequency rhythms are also observed.

Representation of a local layer V circuit is made by reciprocally coupling a fast-spiking excitatory cell, which contains h and T currents, to a fast-spiking inhibitory cell. As shown in Section 3.1, the circuit sustains α-frequency rhythmic activity via postinhibitory rebound spikes in the excitatory cell. The frequency is set by the time courses of the h and T currents rather than by the decay rate of either synaptic type.

To examine synchrony over distance, we incorporate a synaptic conduction delay between two coupled local circuits. Numerical simulations presented in Section 3.2 reveal that this global network model exhibits the same lack of synchrony over distances as is observed experimentally. Analysis of the network presented in Section 3.3 leads to the conclusion that the asynchrony arises from the properties of the h and T currents in the excitatory cells and the strength of distant synaptic connections.

The interplay between the dynamics of the h and T currents and the strengths of synaptic connections creates nonintuitive network behaviors. The stereotypical roles of inhibition and excitation are reversed. Inhibition in the network, which by its nature is thought to slow rhythmic activity, instead increases the firing rate of the excitatory cells. Excitation, usually thought to advance the firing time of cells, instead delays firing in our model. Each of these effects contributes to the desynchronization of the global network.

The role of intrinsic and network properties on synchrony is further clarified in Sections 3.4. For instance, increasing the maximal synaptic conductance of a distant excitatory to excitatory synapse further diminishes our model's ability to sustain synchronous activity. This contrasts markedly with the behavior observed in other network models, where increased levels of network excitation enhance synchrony (Crook et al., 1998; Wong et al., 1986). Also, altering the amount of h current activation in our model affects both the frequency of the network rhythm and the degree of synchrony in the network. In particular, a decrease in the level of h current activation (via a shift in the steady-state values of the h current activation variable) creates a slower network rhythm that is asynchronous at long conduction delays, where the unaltered network could slowly synchronize. Other parameters that shape the domain of conduction delays over which asynchrony occurs are the strength of synaptic connections and the level of depolarizing drive to the inhibitory cells.

Mathematical analysis of the model entails the use of a one-dimensional map, which we show captures the

essential dynamics of the coupled local networks. The geometry of the map (see Section 3.2.1) allows us to make predictions about the behavior of the network as parameters are changed. Numerical simulations in Sections 3.2 and 3.4 confirmed these predictions. Finally, as we show in Section 3.5, simulations of an expanded network model exhibit the same lack of synchrony as the smaller network, and this suggests that the model can be applied to large layer V networks.

2. Methods

In this section we describe the form of the equations used in the numerical simulations. The methods of the mathematical analysis are described in Section 3, Results.

Our local cortical layer V oscillating circuit model consists of two cells—an excitatory pyramidal cell (E cell) and an inhibitory cell (I cell). Both cells are modeled with Hodgkin-Huxley-based current-balance equations:

$$\begin{aligned} C\frac{dV_E}{dt} &= I_L + I_{Na} + I_K + I_T + I_h + I_{\mathrm{GABA_A}} \\ C\frac{dV_I}{dt} &= I_L + I_{Na} + I_K + I_{\mathrm{AMPA}} \\ I_{\mathrm{ion}} &= g_{\mathrm{ion}} m^p h^q (V_{\mathrm{ion}} - V). \end{aligned} \tag{1}$$

Here, C is the membrane capacitance, V_j is the membrane potential of cell j, I_{ion} is an ionic current, g_{ion} is the maximal conductance, m and h are the dynamic activation and inactivation variables for that ion, V_{ion} is the reversal potential for that ion, and p and q are integers.

The local circuit is established by synaptically coupling the cells using model excitatory AMPA (I_{AMPA}) and inhibitory $\mathrm{GABA_A}$ ($I_{\mathrm{GABA_A}}$) synapses.

In addition to sodium (I_{Na}), potassium (I_K) and leak (I_L) currents, the equation for the excitatory cell includes two essential currents that have been observed in layer V pyramidal cells: a hyperpolarization-activated, mixed cation current (I_h) and a low-threshold calcium current (I_T). Each of these inward currents acts to depolarize the cell following hyperpolarization, and they are thought to be important for the generation of α-frequency rhythms in cortex (Castro-Alamancos and Connors, 1996a, 1996b).

The equations for a local circuit are given by Eq. (1) with the intrinsic currents in the numerical simulation modeled as follows:

$$\mathrm{I_{L_{\{e,i\}}}} = g_{L_{\{e,i\}}}\left(E_{L_{\{e,i\}}} - V\right)$$

$$\begin{aligned} \mathrm{I_{Na_{\{e,i\}}}} &= g_{Na_{\{e,i\}}} m^3 h (E_{Na} - V) \\ \alpha_m(V) &= .091(V+38)/(1 - \exp(-(V+38)/5)) \\ \beta_m(V) &= -.062(V+38)/(1 - \exp((V+38)/5)) \\ \alpha_h(V) &= .016\exp((-55. - V)/15) \\ \beta_h(V) &= 2.07/(1 + \exp((17 - V)/21)) \end{aligned}$$

$$\begin{aligned} \mathrm{I_K} &= g_K n^4 (E_K - V) \\ \alpha_n(V) &= .01(-45 - V)/(\exp((-45 - V)/5) - 1) \\ \beta_n(V) &= .17\exp((-50 - V)/40) \end{aligned}$$

$$\begin{aligned} \mathrm{I_T} &= g_T m_T^2 h_T (E_{Ca} - V) \\ m_{T\infty}(V) &= 1/(1 + \exp(-(V+52)/7.4)) \\ \tau_{m_T}(V) &= .44 + .15/(\exp((V+27)/10) \\ &\quad + \exp(-(V+102)/15)) \\ h_{T\infty}(V) &= 1/(1 + \exp((V+80)/5)) \\ \tau_{h_T}(V) &= 22.7 + .27/(\exp((V+48)/4) \\ &\quad + \exp(-(V+407)/50)) \end{aligned}$$

$$\begin{aligned} \mathrm{I_h} &= g_h r (E_h - V) \\ r_\infty(V) &= 1/(1 + \exp((V+75)/5.5)) \\ \tau_r(V) &= 1/(\exp(-14.59 - .086V) \\ &\quad + \exp(-1.87 + .0701V)) \end{aligned}$$

We use standard Hodgkin-Huxley notation for forward and backward rates α_y and β_y of the activation and inactivation variables of each of the currents. $\frac{dy}{dt} = \alpha_y(1-y) - \beta_y y$, or equivalently $\frac{dy}{dt} = (y_\infty - y)/\tau_y$, where $y_\infty = \alpha_y/(\alpha_y + \beta_y)$ and $\tau_y = 1/(\alpha_y + \beta_y)$. Time is in milliseconds.

The synapses in the local network are given by

$$\begin{aligned} \mathrm{I_{AMPA}} &= g_{\mathrm{AMPA}}\mathrm{AMPA}(E_{\mathrm{AMPA}} - V) \\ \mathrm{I_{GABA_A}} &= g_{\mathrm{GABA_A}}\mathrm{GABA_A}\left(E_{\mathrm{GABA_A}} - V\right) \\ \frac{d\mathrm{AMPA}}{dt} &= 1.1tr(e_{sp})(1 - AMPA) - .19AMPA \\ \frac{d\mathrm{GABA_A}}{dt} &= 5tr(i_{sp})(1 - \mathrm{GABA_A}) - .18\mathrm{GABA_A} \\ tr(\{e,i\}_{sp}) &= \mathrm{Heaviside}(-1.0\{e,i\}_{sp}), \end{aligned}$$

where $\{e, i\}_{sp} < 0$ for 1 millisecond when the voltage of the presynaptic cell crosses a threshold, $V_{\text{threshold}}$.

To investigate networks coupled over long spatial distances, we synaptically couple two of the local two-cell circuits described above. Physical distance between the local circuits is modeled using a time delay, δ, in synaptic coupling, with larger delays corresponding to a greater distance. The synapses between distantly coupled circuits are weaker than the synapses within local circuits. However, since we are considering individual neurons that make patches of direct monosynaptic connections with other neurons several millimeters distant, we use a fixed coupling strength between distantly coupled cells (regardless of distance). This is justified in that there seems to be no difference in the synaptic connections made between neurons in patches that are close together (such as 1 mm) versus patches that are further apart (such as 7 mm).

We study only long-range connections from excitatory cells (Hirsh and Gilbert, 1991). For our initial analysis of the global network, the network configuration contains only distant excitatory to inhibitory AMPA synapses (modeled the same as for the local circuit above). Figure 1 depicts this four-cell global network configuration. The addition of distant excitatory to excitatory AMPA synapses is investigated in Section 3.4.2.

The standard values of the parameters, for the four-cell global network, are given below. The capacitance, C, of each cellular membrane is set at 1 μF/cm^2 (F = Farad). The maximal conductances in mS/cm^2 (S-Siemens—that is, Mhos.) are $g_{L_e} = 0.07$, $g_{L_i} = 0.05$, $E_{L_e} = -75$, $E_{L_i} = -60$, $g_{\text{Na}_e} = 60$, $g_{\text{Na}_i} = 100$, $E_{\text{Na}} = 45$, $g_{\text{K}} = 30$, $E_{\text{K}} = -90$, $g_{\text{T}} = 2.2$, $E_{\text{Ca}} = 125$, $g_h = 0.08$, $E_h = -43$, $g_{\text{AMPA}} = 0.2$ (E to I within a local two-cell circuit) $= 0.1$ (E to I between distant local circuits) $= 0.05$ (E to E between distant local circuits), $E_{\text{AMPA}} = 0$, $g_{\text{GABA}_\text{A}} = 0.5$ (I to E within a local two-cell circuit; there are no distant inhibitory connections), $E_{\text{GABA}_\text{A}} = -80$, $V_{\text{threshold}} = 0$. The various parameter values used in our analysis came from a variety of sources (Destexhe et al., 1998; Golomb and Amitai, 1997; Mainen et al., 1995; McCormick and Huguenard, 1992; Pinsky and Rinzel, 1994).

All simulations are performed using G.B. Ermentrout's package for solving ODEs—XPPAUT. This package is available from ftp://ftp.math.pitt.edu/-pub/bardware. The usual method of integration is a fourth-order Runge-Kutta method.

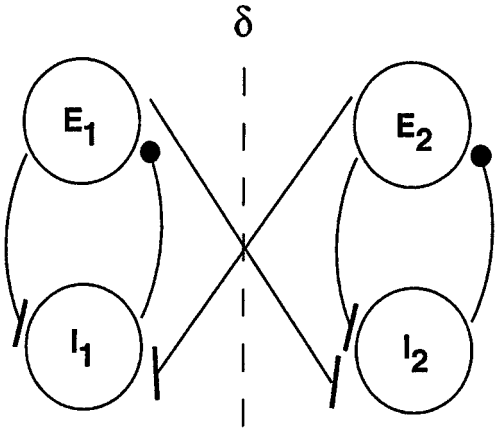

Figure 1. The global network configuration: Two 2-cell local networks connected via distant E to I AMPA synapses with a time delay, δ, in synaptic propagation between networks.

3. Results

3.1. Generation of Local α-Frequency Rhythms

We begin by describing the intrinsic and network mechanisms that generate sustained α-frequency rhythms within the local two-cell networks. The initial analysis considers only local reciprocal coupling (E to I, and I to E); local recurrent excitatory or inhibitory coupling is discussed in Section 3.4.3.

The after-hyperpolarization dynamics of the h and T currents in the excitatory cell make sustained rhythmic activity possible. Figure 2 shows the progression from

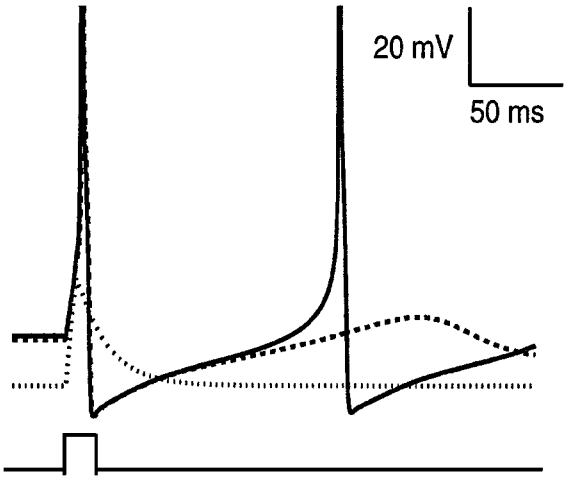

Figure 2. Progression to a rebound spike in an excitatory cell after an initial 5 ms depolarization. *Light dotted curve*: $g_h = g_T = 0$; *dark dashed curve*: $g_h = 0.07$; $g_T = 1.9$; *solid curve*: $g_h = 0.08$, $g_T = 2.2$. Increasing g_h alone was not sufficient to generate sustained rhythmic activity. Increasing g_T alone was sufficient, as long as $g_T > 2.3$. For all curves $g_{\text{GABA}_\text{A}} = 0.5$, $g_{\text{AMPA}} = 0.2$.

a single spike to rhythmic activity in a local excitatory cell via an increase in the maximal h and T current conductances (g_h and g_T). Following an initial spike in both of the local cells, the inhibitory cell briefly hyperpolarizes the excitatory cell, activating I_h and deinactivating I_T. At low maximal conductance levels the excitatory cell simply returns to rest. As the conductance levels increase, the inward currents cause the excitatory cell to generate a rebound spike. It is this rebound spike that drives the inhibitory cell and thus sustains rhythmic activity. The level of excitation to the local I cell is chosen to produce a single I-spike per cycle in the E-I network. Using physiologically realistic parameter values, the sustained rhythm has a frequency between 7 to 14 Hz and depends primarily on the dynamics of I_h and I_T (Bazhenov et al., 1998; Destexhe et al., 1993; Golomb and Amitai, 1997; Mainen et al., 1995; McCormick and Huguenard, 1992; McCormick and Pape, 1990b).

3.2. *Synchronization Properties of α-Frequency Rhythms over Spatial Distances in Cortex*

To examine properties of synchronization, we consider a pair of two-cell local oscillating circuits coupled together to form a global four-cell network, as described in Section 2, Methods.

We construct a one-dimensional map that captures the essential dynamics of the global coupled network. From the map, we make predictions about the ranges of delays, δ, and initial phase lags of the oscillators, $\triangle$, over which the network does or does not synchronize (synchrony is measured between E_1 and E_2 and is defined to be a zero phase lag steady state between these two cells), and about rates of synchronization and desynchronization. We then give numerical simulations verifying these predictions. As we show in this section, under a wide range of conditions the two local networks, connected via long-distance excitatory to inhibitory AMPA synapses, do not synchronize. Furthermore, as we show in Section 3.4.2 the addition of long-distance excitatory to excitatory connections increases the regimes under which there is desynchronization.

3.2.1. Construction of the One-Dimensional Map. It is useful to study the global network dynamics by developing a one-dimensional map H that describes the progression of the network toward or away from a synchronous state. We label the excitatory and inhibitory cells by E_1, I_1 and E_2, I_2, respectively. Following Ermentrout and Kopell (1998), let

$$\begin{aligned} t_1 &= \text{time when } E_1 \text{ fires,} \\ t_2 &= \text{time when } E_2 \text{ fires,} \\ \bar{t}_1 &= \text{next time when } E_1 \text{ fires,} \\ \bar{t}_2 &= \text{next time when } E_2 \text{ fires.} \end{aligned}$$

After E_1 fires, it takes an amount of time equal to $t_2 + \delta - t_1$, for E_1's circuit to receive excitatory input from E_2. Thus,

$$\bar{t}_1 = t_1 + f(t_2 + \delta - t_1),$$

where f is a function describing the wait to firing after receiving excitation; we shall determine f numerically from the underlying Hodgkin- Huxley equations. Since the E cells and coupling are identical, $\bar{t}_2$ satisfies

$$\bar{t}_2 = t_2 + f(t_1 + \delta - t_2)$$

for the same function f.

We are interested in the synchronization properties of the entire network, and, hence, we define $\triangle := t_2 - t_1$, the difference in spike times of the two units. The synchronized state corresponds to $\triangle = 0$. We now determine the conditions under which $\triangle = 0$ is a stable state and, hence, under which network synchrony will be achieved.

Let $\bar{\triangle} := \bar{t}_2 - \bar{t}_1$. From the above definitions of $\bar{t}_1$ and $\bar{t}_2$, we obtain

$$\begin{aligned} \bar{\triangle} &= t_2 - t_1 + f(t_1 + \delta - t_2) - f(t_2 + \delta - t_1) \\ &= \triangle + f(-\triangle + \delta) - f(\triangle + \delta) \\ &\equiv H_\delta(\triangle). \end{aligned} \tag{2}$$

For a fixed δ, the function H_δ is a one-dimensional map describing the difference, $\bar{\triangle}$, in spike time at each cycle in terms of the difference, $\triangle$, at the last cycle. Since $H_\delta(0) = 0$, a synchronous solution exists as a fixed point of this map.

To evaluate the stability of this synchronous state, we calculate the derivative of H_δ with respect to $\triangle$ and evaluate this derivative at $\triangle = 0$:

$$\begin{aligned} H'_\delta(\triangle) &= 1 - f'(-\triangle + \delta) - f'(\triangle + \delta) \\ H'_\delta(0) &= 1 - 2f'(\delta). \end{aligned}$$

By standard results about one-dimensional maps (Devaney, 1992), synchrony is stable when $|H'_\delta(0)| <$

1 and therefore only when

$$0 < f'(\delta) < 1.$$

In the remaining cases, when either $f' < 0$ or $f' > 1$, synchrony is an unstable fixed point of H_δ, and when $f' = 0$ or $f' = 1$, synchrony is neutrally stable. Thus, to understand the conditions under which synchrony is stable or unstable, it suffices to examine the shape of the function f.

3.2.2. Numerical Computation of f and Predictions. Figure 3A shows the function f generated from a single oscillating circuit receiving imposed inputs as it would as part of the network configuration of Fig. 1. Assuming E_1 fires first at time $t_1 = 0$, the points on the graph of f give the next time E_1 fires. Note that f is a function of $\triangle + \delta$. Figure 3A was labeled setting $\triangle = 0$, the case for the synchronous solution. Thus, the values along the x-axis, which represent the arrival times of distant pulses to the local oscillating circuit, are given solely by the propagation delay δ. The dotted horizontal line denotes the next time E_1 fires in the absence of distant inputs (that is, the intrinsic period of E_1). Along the x-axis, f is broken into five regions according to its slope as described in Table 1.

Referring to f', as described in Table 1, we make the following predictions based on the analysis of Section 3.2.1. The flat shape of f in Region 1 indicates that the firing of an excitatory cell is not affected by inputs arriving during the first 7 ms of its period. Thus, for sufficiently small differences in initial conditions, $\triangle$, synchrony will be neutrally stable. Since f' is less than zero in Region 2a (that is, for delays $7 < \delta < 10$), the network will not exhibit synchronous behavior in that region. By contrast, in Region 3b the global network will be able to synchronize as long as $\triangle$ is small. However, the time to synchrony is long when f' is small, and when synchrony does not occur quickly it may be physiologically irrelevant. Finally, in the intermediate regimes (Regions 2b and 3a) where f' is almost zero, we would expect very slow desynchronization or synchronization with a transition as we vary δ. As we show in Section 3.4, changes of parameters can change the boundaries of the above regions or even the slopes but do not change them to produce fast synchronization in any range of δ.

Table 1. Geometry of f in Fig. 3A and predictions on the stability of the synchronous solution of the global network behavior assuming $\triangle$ starts close to zero. The separation of Regions 2b and 3a represents the *numerical* transition from asynchrony to synchrony, as is described in Section 3.2.3 and further verified in Section 3.3.2.

Region	Time of Arrival (δ)	Slope of f	Synchronous Sol.
1	0–7	$f' = 0$	Neutrally stable
2a	7–10	$f' < 0$	Unstable
2b	10–12	$f' \approx 0$	Almost neutrally stable
3a	12–15	$f' \approx 0$	Almost neutrally stable
3b	15–25	$0 < f' < 0.25$	Stable

3.2.3. Network Simulations. We tested the synchrony of the global network in a series of simulations varying δ and $\triangle$. For $\triangle$ close to zero the predictions on the stability of synchrony, as outlined in Table 1, were confirmed by all of the numerical simulations. In particular, for each fixed δ, if the values of both $(-\triangle + \delta)$ and $(\triangle + \delta)$ remained within the same region along the x-axis then the slope of f accurately predicted the network behavior. However, for values of $\triangle$ such that the values of $(-\triangle + \delta)$ and $(\triangle + \delta)$ lay in two different regions along the x-axis, transient dynamics can be complex and of long duration. However, even in that situation, the map H_δ correctly predicts numerical values of $\bar{\triangle}$ on a cycle by cycle basis.

In Region 1 ($\delta < 7$), synchrony was neutrally stable. For all network simulations in this region, if $\triangle$ was chosen such that $(-\triangle + \delta)$ and $(\triangle + \delta)$ remained less than 7 ms, then $\bar{\triangle} = \triangle$, and hence solutions that are initially nonsynchronous remain nonsynchronous, and solutions initially synchronous remain synchronous. In particular, a common initial input can create synchronous behavior. Finally, for all larger $\triangle$, asynchronous behavior was observed.

In Region 2a ($7 < \delta < 10$), asynchrony (unstable synchrony) occurred for all values of $\triangle$. A representative case is shown in Fig. 3B.

In Region 2b ($10 < \delta < 12$), for small $\triangle$ such that $(-\triangle + \delta)$ and $(\triangle + \delta)$ remained between 10 ms and 12 ms, a slow approach to an asynchronous state occurred. For larger $\triangle$, asynchrony was observed.

In Regions 3a and 3b ($12 < \delta < 25$), synchrony occurred for all $\triangle$ tested, with the rate of approach to synchrony predicted correctly by the slope of f—that is, a smaller slope implies a slower approach. In Fig. 3C, we show a network with $\triangle = 1$ ms, which becomes synchronous in approximately three cycles. However, for larger $\triangle$, the synchronization was slower and could exceed 5 seconds.

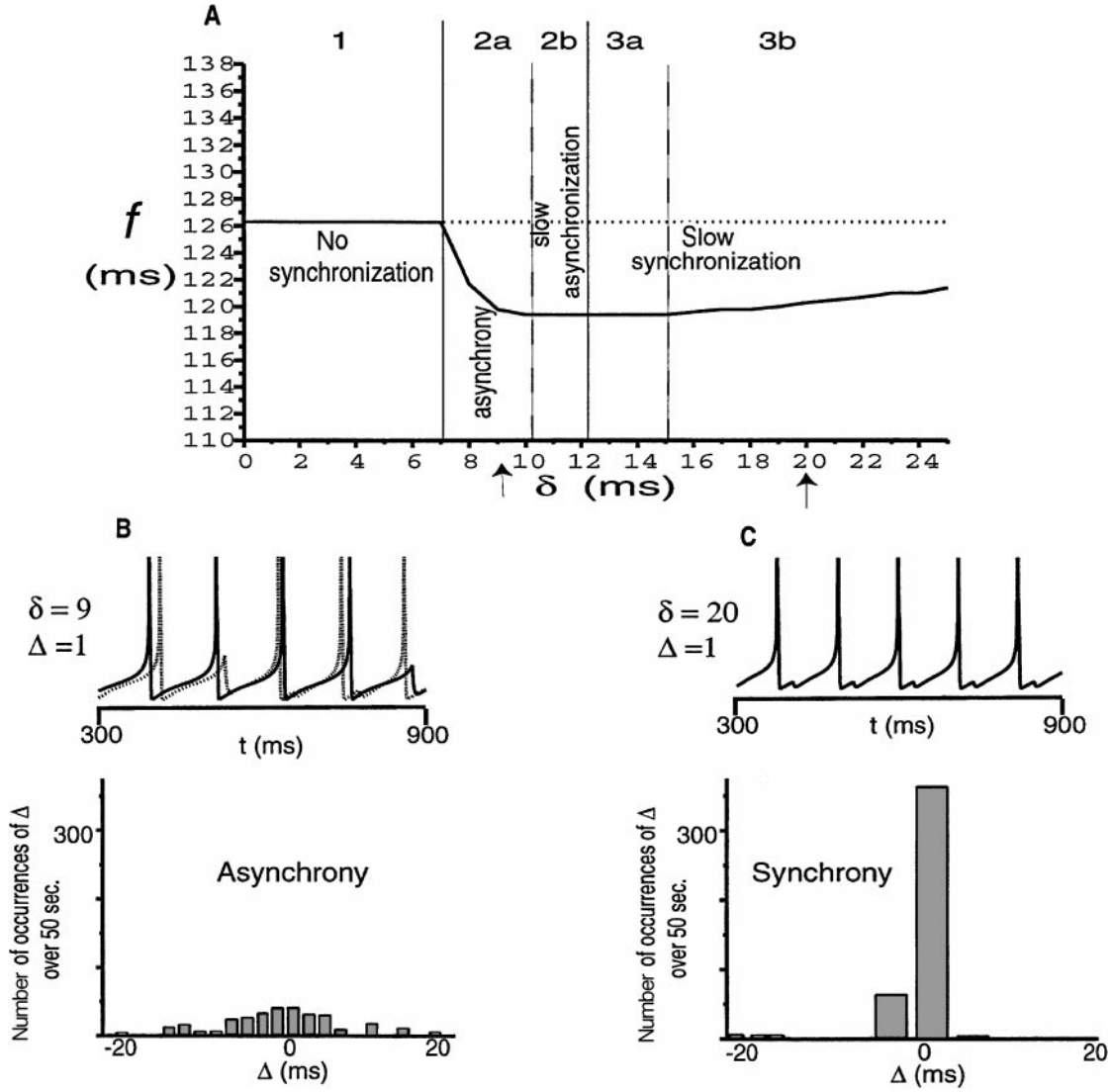

Figure 3. **A:** Graph of f generated under the network configuration of Fig. 1. *x-axis*: $\delta =$ the arrival time of a distant pulse to an oscillating local circuit under the condition $\triangle = 0$; *y-axis*: next firing time of E_1 assuming the first firing time, t_1, equals 0. The dotted horizontal line at ≈ 126 ms represents the period of the excitatory cell without any external input. Regions 1, 2a/2b, and 3a/3b separate the graph of f according to the numerical occurrence of synchrony in the network, these results are summarized in each region. The separation within Regions 2 and 3 are present for the sake of discussion of changes in slope. **B and C:** *Top frame:* Voltage traces of E_1 (solid curve) and E_2 (dashed curve) over 600 ms. *Bottom frame:* Corresponding histograms giving the number of occurrences of specific differences in spike times, $\triangle$, of E_1 and E_2 over 50 seconds. **B:** $\triangle = 1$ and $\delta = 9$. The network does not reach a steady state. Thus, the figure label states that asynchrony occurs. **C:** $\triangle = 1$ and $\delta = 20$. Synchrony occurs (in approximately three cycles) and persists. For all functions f generated in this article, when one oscillating unit is hit with a pulse from another it returns to its limit cycle within two periods.

The results of this section reveal that the α-frequency rhythms desynchronize over long cortical distances. However, these results also demonstrate that α-frequency rhythms can be synchronized over short distances in the presence of common (that is, simultaneous) input.

3.3. Origin of Asynchrony

In this section, we dissect the features of the model that control the shape of f and hence are responsible for the lack of synchronization over distances reported in Section 3.2. As we shall see, both inhibition and

excitation behave in nonintuitive ways; local inhibition advances the firing time of the local excitatory cells, whereas distant excitation delays it.

3.3.1. A Closer Look at the Shape of f. In this section, we investigate the determinants of the endpoints of each region and the slope of f within each region. We show that the distant network connections, their effect of the generation of spikes in the inhibitory cells, and the intrinsic kinetics in the excitatory cells all affect the shape of f, sometimes in a nonintuitive way. Each geometrically distinct region described in Table 1 is analyzed separately.

Region 1 In this region the slope of f remains equal to zero and small differences in initial conditions remain. The firing time of the excitatory cell (E-cell) is unaffected by input arriving in the first 7 ms. As shown in Fig. 4A, the E-cell voltage traces (solid curves) with $\delta = 0, 4$, and 7 ms lie directly on top of one another.

The only way distant excitatory to inhibitory pulses can affect the local E-cell is via the $GABA_A$ synapse, which is activated only when the local I-cell spikes. When δ is between 0 to 7 ms, however, the local I-cell is still in a refractory state, and hence there are no "doublets" in the I-cell (dashed curves in Fig. 4B). Therefore, the E-cell is unaffected by external input and f remains flat. As we will see in Section 3.4.2, this situation changes dramatically with the inclusion of distant excitatory to excitatory connections.

Region 2a The slope of f in this region is negative, and only asynchronous solutions were observed in the global network. In Fig. 4B we see that, when $\delta = 8$ ms, the distant excitatory to inhibitory input arrives at the local I-cell late enough in its period to create a second postsynaptic inhibitory spike (doublet). This second postsynaptic inhibitory spike hyperpolarizes the E-cell causing it to spike significantly sooner than it did without the hyperpolarization (see Fig. 4B). Thus, there is a steep drop of f, at $\delta = 8$ ms, in Region 2a. According to the theory above, this negative slope implies asynchrony. Note that in the context of this model, the doublet spike now creates asynchrony, not synchrony as in the γ and β rhythms (Ermentrout and Kopell, 1998; Kopell et al., 2000; Traub et al., 1996, 1999).

This nonintuitive decrease in firing time after receipt of local inhibition is a direct result of the hyperpolarization-activated inward currents in the

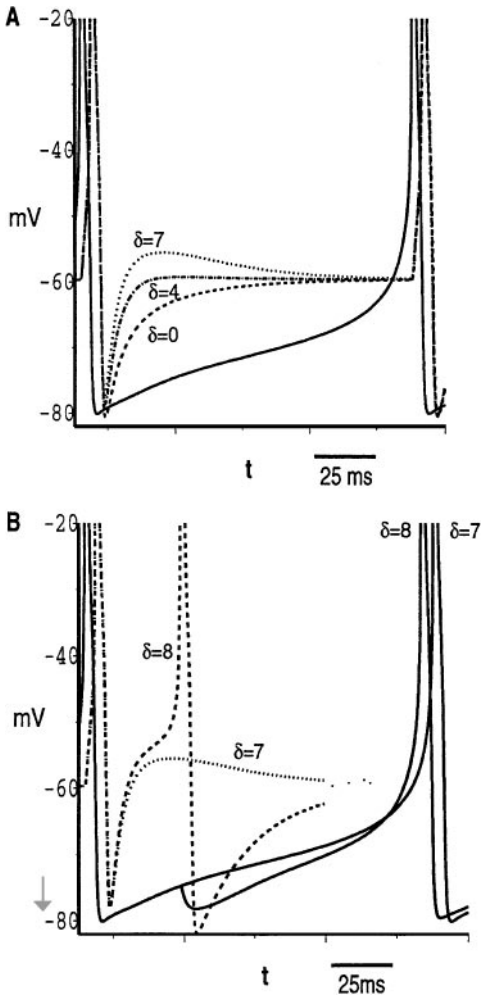

Figure 4. Dynamics in Regions 1 and 2a. Displayed are several voltage versus time cycles of the local excitatory (solid curves) and inhibitory (dashed curves) cell, which result from distant excitatory inputs arriving to the inhibitory cell at precisely **A** 0 ms (dashed), 4 ms (dashed-dotted) and 7 ms (dotted) or **B** 7 ms (dotted) and 8 ms (dashed) into the local excitatory cell's period. Note that an input arriving at 0 ms actually means no input arrived to the local circuit. The gray arrow along the y-axis in Fig. 4B signifies the decrease in voltage of the excitatory cell resulting from a spike in the inhibitory cell.

excitatory cell. The second inhibitory spike hyperpolarizes the E-cell from approximately -75 mV to -80 mV, as indicated by a gray arrow along the y-axis in Fig. 4B, and we now explain why this causes the excitatory cell to fire significantly sooner.

Figure 5 illustrates the effect of the hyperpolarization on the inward currents. Let r represent the activation variable of the h current and m_T and h_T the activation and inactivation variables of the T current. Figures 5A and 5B present the voltage dependent steady state

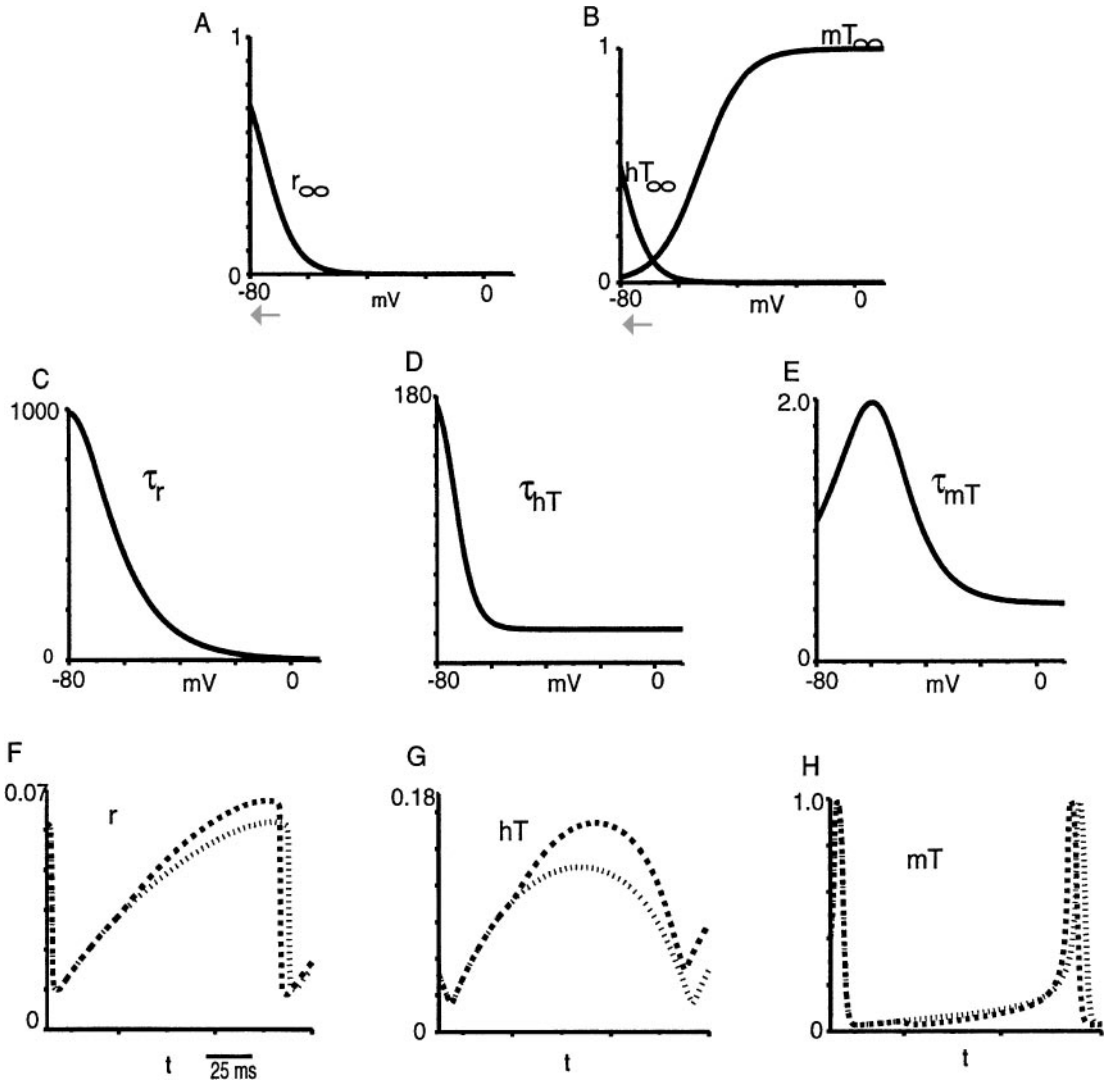

Figure 5. **A:** Graph of the steady-state values, $r_\infty(V)$, for the activation variable of the h current. **B:** Graphs of the steady-state values, $h_{T\infty}(V)$ and $m_{T\infty}(V)$, for the inactivation and activation variables of the T current, respectively. **C:** Graph of the time constant, τ_r, for the activation of the h current. **D:** Graph of the time constant, $\tau_{h_T}(V)$, for the inactivation of the T current. **E:** Graph of the time constant, $\tau_{m_T}(V)$, for the activation of the T current. **F:** Traces of the activation variable, r, of the h current corresponding to distant excitatory inputs arriving to the inhibitory cell at precisely 7 (light dotted curve) and 8 (dark dashed curve) ms into the local excitatory cell's period (that is, $\delta = 7$ ms and $\delta = 8$ ms). **G:** Corresponding traces of the inactivation variable, h_T, of the T current. **H:** Corresponding traces of the activation variable, m_T, for the T current. The gray arrows along the axes in **A** and **B** signify the decrease in voltage of the excitatory cell, which results from a spike in the inhibitory cell when $\delta = 8$ ms, as also depicted in Fig. 4B.

values of h current activation ($r_\infty(V)$), T current activation ($m_{T\infty}(V)$), and T current inactivation ($h_{T\infty}(V)$). Figures 5C, 5D, and 5E present their voltage-dependent time constants. In particular, note that at hyperpolarized voltage levels, the h current activates while the T current both deactivates *and* deinactivates. Notice also that h current activation and T current inactivation change at rates 1000 and 100 times slower than T current activation.

Thus, when the E-cell is hyperpolarized by synaptic inhibition ($\delta = 8$ ms), r and h_T slowly increase, while m_T rapidly decreases (see dark dashed curves in Figs. 5F, 5G, and 5H). Despite this deactivation of the T current, the net result of the increase in h current activation, T current deinactivation, and the decay of the inhibition is to cause the E-cell to depolarize more rapidly than when no hyperpolarization ($\delta = 7$ ms; light dashed curves in Figs. 5F, 5G, and 5H) occurred. As

the voltage rises, m_T rises rapidly, further depolarizing the cell. Thus, it is the *combined* depolarizing effects of both I_h and I_T, induced by the second inhibitory spike, that allow the E-cell to spike sooner when $\delta = 8$ ms than when $\delta = 7$ ms.

As the delay, δ, increases from 8 ms to 10 ms, the distant excitatory inputs arrive at the local I-cell near the end of its refractory period but early enough to combine with the excitatory influence of the local E-cell. This causes the I-cell to fire sooner as δ increases. Correspondingly, the E-cell also fires sooner, as described above, and f continues to decrease. More analysis of this region, using maps more detailed than those in Section 3.2.1, is given in the next section (Section 3.3.2).

Regions 2b and 3a The slope of f in Regions 2b and 3a is approximately zero, and network conditions in these regions produce slow approaches to asynchrony or synchrony, respectively. As the delay, δ, increases from 10 ms to 15 ms, the distant excitatory inputs arrive at the local I-cell as it is leaving its refractory state and less of the EPSP from the local E-cell remains. These two effects approximately cancel each other, and the second inhibitory spike occurs at roughly the same time for all delays $10 < \delta < 15$ ms, therefore evoking similar responses in the E-cell for all such delays. Thus, f remains almost flat in Regions 2b and 3a. The distinction between Regions 2b and 3a will be further analyzed in Section 3.3.2.

Region 3b The slope of f in Region 3b is positive and less than one, and network conditions in this region produce synchronous solutions. In this region, the distant excitation arrives at the local I-cell when there is no remaining refractoriness of the I-cell or remaining synaptic current from the previous local EPSP. Hence, the I-cell fires at a fixed time after receipt of excitation, independent of δ. This causes the E-cell to also fire later as δ increases, producing a positive slope for f. However, the presence of the h and T currents, which advance the firing time, results in the slope of f being less than 1 (actually less than 0.25, as determined numerically).

3.3.2. Region 2: Inhibition Generates Earlier Firing Times. In this section, we further analyze the roles of the local E and I cells in producing asynchrony in the network configuration of Fig. 1 for conductance delays $8 < \delta < 12$. We focus on this region since it is nonintuitive that inhibition leads to earlier firing times in the local E-cell. In particular, we follow Ermentrout and Kopell (1998) and split the map H_δ (see Section 3.2.1) into two components that individually encode critical information about the spike times of the I and E cells, respectively.

Near synchrony, an I-cell receives two excitatory inputs, one from its local E- cell and one from the distant E-cell. The local excitatory input arrives first and causes the I-cell to spike. Let T_I denote the amount of time it takes the inhibitory cell to spike again, after it receives the distant excitatory input—that is, $T_I = T_I(\phi)$, where $\phi = \triangle + \delta$.

Also near synchrony, each E-cell receives two inhibitory pulses from its local I-cell. Considering E_1 as the local E-cell, each pulse arrives at E_1 via one of the following synaptic paths:

$$\text{Path 1:} \quad E_1 \Rightarrow I_1 \Rightarrow E_1.$$
$$\text{Path 2:} \quad E_2 \Rightarrow I_1 \Rightarrow E_1.$$

Let θ denote the difference in the arrival times along Paths 1 and 2. The map $T_E = T_E(\theta)$ is defined to be the amount of time, after the second inhibitory input is received, for E_1 to fire.

In particular, the times for the inhibitory inputs to arrive at E_1 via the two paths can be determined as follows. For Path 1, cell E_1 first fires at time t_1. Then, in response, it takes an amount of time, t_{ei}, for I_1 to fire. Along Path 1, the inhibitory input from I_1 arrives at E_1 at time $t_1 + t_{\text{ei}}$. Along Path 2, cell E_2 fires at time t_2, and there is a delay of time δ before cell I_1 receives this input. This input to I_1 is precisely the second input to the local I-cell discussed in the previous paragraph. Therefore, I_1 will fire again after a time given by $T_I(\phi)$ and hence the time at which E_1 receives inhibitory input via Path 2 is $t_2 + \delta + T_I(\phi)$. To summarize:

Path 1: Arrival time is $t_1 + t_{ei}$.

Path 2: Arrival time is $t_2 + \delta + T_I(\triangle + \delta)$.

Thus,

$$\begin{aligned}\theta &= t_2 + \delta + T_I(\triangle + \delta) - (t_1 + t_{ei}) \\ &= \triangle + \delta - t_{ei} + T_I(\triangle + \delta).\end{aligned}$$

In this new context, we now recalculate $H_\delta(\triangle) = \bar{\triangle} = \bar{t}_2 - \bar{t}_1$ as follows. The time $\bar{t}_1$ at which E_1 fires

in the next cycle is given by

$$\begin{aligned}\bar{t}_1 &= \text{time at which the inhibitory input via Path 2 arrives} + T_E(\theta)\\ &= t_2 + \delta + T_I(\triangle + \delta) + T_E(\triangle + \delta - t_{ei} + T_I(\triangle + \delta)).\end{aligned}$$

A similar formula holds for $\bar{t}_2$, with indices 1 and 2 reversed and $\triangle$ changed to $-\triangle$. Therefore,

$$H_\delta(\triangle) = -\triangle + F_\delta(-\triangle) - F_\delta(\triangle),$$

where

$$F_\delta(\triangle) = T_I(\triangle + \delta) + T_E(\triangle + \delta - t_{ei} + T_I(\triangle + \delta)).$$

The map F contains the same information as the map f introduced in Section 3.2.1, and it can be shown that $F_\delta(\triangle) = f(\triangle + \delta) - (\triangle + \delta)$. However, the parsing of F_δ into T_I and T_E allows us to look more closely at the individual effects of excitation and inhibition.

As before, the synchronous solution, $\triangle = 0$, is stable if $|H'_\delta(0)| < 1$. Using methods similar to those in Section 3.2.1 for the map f, we find here that synchrony is stable if $-1 < F'_\delta(0) < 0$ and unstable if $F'_\delta(0) < -1$ or $F'_\delta(0) > 0$. When $\triangle = 0$, we can consider both T_I and T_E to be functions of the parameter δ, and so $F'_\delta(0) = T'_I(\delta) + \tilde{T}'_E(\delta)[1 + 2T'_I(\delta)]$, where $\tilde{T}_E(\delta) = T_E(\delta - t_{ei} + T_I(\delta))$. Figures 6A and 6B show numerically generated graphs of $T_I(\delta)$ and $\tilde{T}_E(\delta)$, for $\delta > 8$ ms. Figure 6C shows $F'_\delta(0)$ and its components $T'_I(\delta)$ and $\tilde{T}'_E(\delta)$, as obtained numerically using Figures 6A and 6B. According to the graph of F'_δ, synchrony is unstable for $8 < \delta < 12$ and stable for $\delta > 12$.

A critical feature of our model is that the local E-cells have h and T currents. Hence, the map $\tilde{T}_E(\delta)$ obtained here differs qualitatively from the map $\tilde{T}_E(\delta)$ obtained for cells with only I_L, I_{Na}, and I_K. We may compare, for instance, the work of Ermentrout and Kopell (1998), where the I and E cells are modeled using only those three currents. There, when $\triangle = 0$, both $T'_I(\delta)$ and $\tilde{T}'_E(\delta)$ are less than or close to zero for all values of δ in which they exist. Our $T'_I(\delta)$ is also negative for all values of δ shown (see Fig. 6C), since our I-cell is also modeled using the standard spiking currents. However, the additional h and T currents in our local E-cells create a significant change in $\tilde{T}'_E(\delta)$, which is now positive for $8 < \delta < 12$. It is the positive contribution of $\tilde{T}'_E(\delta)$ that allows the product $\tilde{T}'_E(\delta)[1 + 2T'_I(\delta)]$ to be negative, which in turn implies that $F'_\delta(0) < -1$ for $8 < \delta < 12$. We conclude that it is the additional intrinsic kinetics of the E-cell, arising from the inclusion of I_h and I_T, that generate asynchronous behavior in the full network.

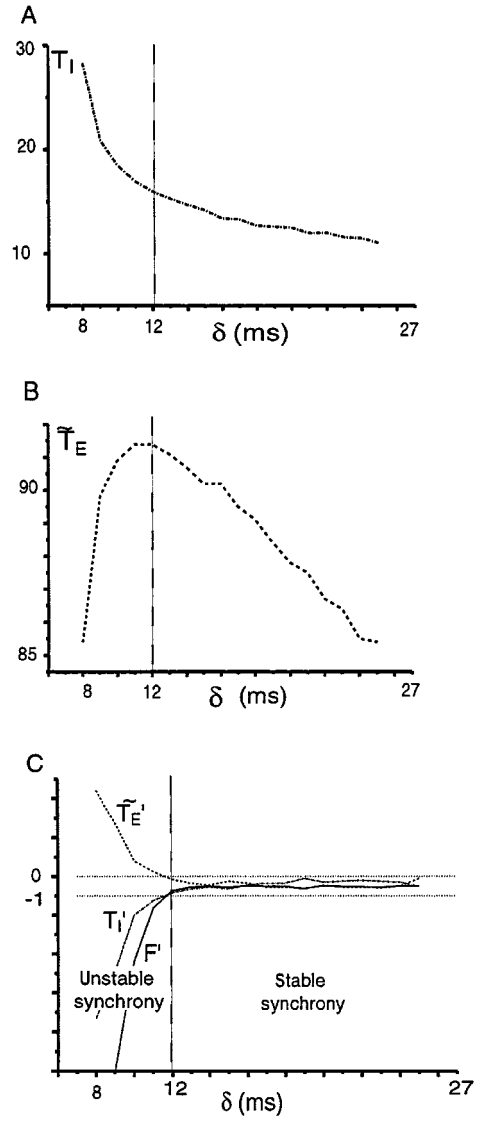

Figure 6. **A** and **B:** Graphs of $T_I(\delta)$ and $\tilde{T}_E(\delta)$, for $\delta > 8$ ms. **C:** Corresponding graphs of $T'_I(\delta)$, $\tilde{T}'_E(\delta)$, along with $F'_\delta(0) = T'_I(\delta) + \tilde{T}'_E(\delta)[1 + 2T'_I(\delta)]$. According to the graph of F', synchrony will be unstable when $\delta < 12$ ms and stable when $\delta > 12$ ms. All graphs were generated with the same parameter values used to generate f in Fig. 3.

For completeness, we note that the unstable synchrony region predicted by this graph ends at $\delta = 12$ ms, which is the boundary between Regions 2b and 3a in

Fig. 3A. This confirms our previous conclusion that $\delta = 12$ ms marks the point where the behavior of the network that starts close to synchrony changes from being slowly asynchronous to being slowly synchronous in the numerical simulations (see Section 3.2.3).

3.4. Effects of Changing System Parameters

In Section 3.3, we showed that the shape of f, and hence the occurrence of synchrony in the network, is dependent on the parameters in our network model. Here, we investigate the effects of changing some of the parameters that play a dominant role in defining f's shape.

3.4.1. Effects of Modulating the h Current. The h current is known to be strongly susceptible to neural modulation (McCormick and Pape, 1990a). Here we analyze qualitatively the influence of modulating the h current on the network synchrony. We find that decreasing the h current steady-state activation level results in fewer conditions under which network synchrony occurs. In particular, asynchrony occurs at long conduction delays at which the unmodulated network exhibits slow synchronization.

This difference in the network is predicted by the changes of the map f resulting from h current modulation (see Fig. 7A). As in the unmodulated network, delays of at least 8 ms generate a second inhibitory spike, causing f to decrease for δ between 7 and 8 ms, as described in Section 3.3.1.

For delays, δ, between 8 to 10 ms, the second inhibitory spike arrives at earlier times in the period of the E-cell as in the unmodulated network (see Section 3.3.1). Hence, the voltage value of the excitatory cell at the instant the second inhibitory spike arrives decreases with increased δ (see Fig. 4B). Thus, the initial *rate* of h activation ($\tau_r(V)$) decreases (see Fig. 5C). In the unmodulated network, this effect is negligible and f continues to decrease. However, in the modulated network, this decrease in *rate*, in addition to the fact that the maximum that r can attain is decreased, are sufficient to keep r from reaching levels where the excitatory cell is depolarized enough to spike sooner; instead it spikes later as δ increases from 8 to 10 ms. Hence, f increases ($0 < f' < 0.6$). In this region, all simulations verified that the network could synchronize but only in the very limiting case where $\triangle$ was chosen small enough so that $8 < \triangle + \delta < 10$.

For delays $10 < \delta < 15$, the modified and unmodulated networks are similar. The second inhibitory spike arrives at the excitatory cell at approximately the same time with delays $10 < \delta < 15$. Hence, there is no noticeable change in the firing time of the excitatory cell and both functions f remain roughly flat.

Once the conduction delay is as long as $\delta = 15$ ms, the second inhibitory spike in each network begins to arrive *later* in the period of the excitatory cell, as described in Section 3.3.1. Hence, its voltage value at the instant the inhibition arrives is larger (see Fig. 4B). Thus, the initial increase in h current activation occurs more quickly (since $\tau_r(V)$ is smaller). In the unmodulated network, this effect is negligible and f increases with a slope less than one (see Section 3.3.1). However, in the modulated network, the initial *rate* of h activation plays a dominant role in defining the slope of f for $\delta > 15$ ms. Here, although the values that r attains are reduced, as δ increases past 15 ms the initial *rate* of h activation gradually increases enabling r to reach levels that are sufficient to change the spike time of the excitatory cell (that is, cause it to spike sooner). Hence, as δ increases, f gradually decreases.

All of the network simulations conducted with delays of $\delta \geq 10$ ms produced asynchrony. To see results from the modulated network, which contrast those from the unmodulated network, compare Fig. 3C to Fig. 7B ($\delta = 20$ ms).

3.4.2. Effects of Adding Distant Excitatory to Excitatory Connections. Until this point, the only distant connections we have considered are from E to I cells. The effects of E to E connections on synchronization are subtle. In some simple systems, such connections prevent synchronization (Hansel et al., 1995; Van Vreeswijk et al., 1994). In other systems, notably if the cells have adapting currents, the E to E connections can be synchronizing (Crook et al., 1998); E to E connections have also been shown to facilitate synchrony in some bursting cells (Wong et al., 1986).

In our system, E to E connections, in combination with the inward I_h and I_T currents, act to further desynchronize network activity. In particular, with the addition of long distance E to E coupling (in the network configuration of Fig. 1) of strength greater than 0.025 units, the subsequent map f (see Fig. 8A) displays a slope larger than one for $0 < \delta < 7$ ms, indicating that synchrony is now unstable for this range of delays. (When the coupling strength is less than 0.025,

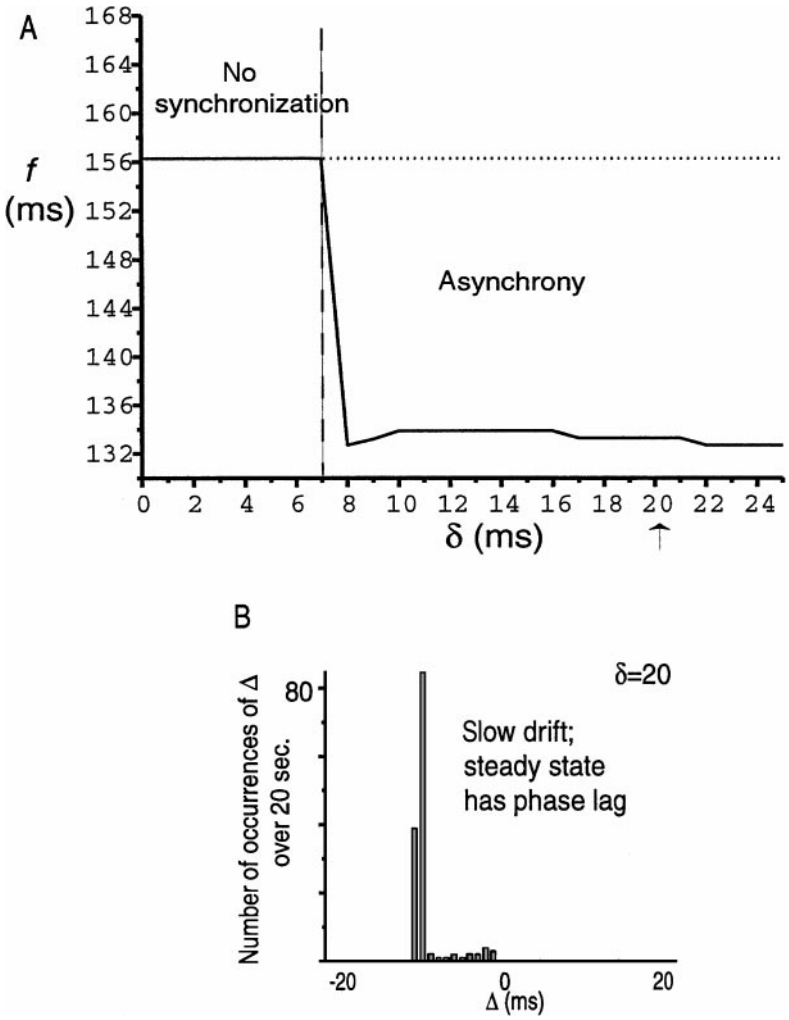

Figure 7. **A:** Graph of f generated with less h current activation, by shifting $r_\infty(V)$ 10 mV to the left (see Fig. 5A). The dotted horizontal line at $\approx$ 156 ms represents the period of the excitatory cell without any distant input. Each axis has been cropped; the entire phase of the local circuit (0 to 156 ms or $\approx$ 6.5 Hz, a slower rhythm) is not shown. The graph is separated into two regions. In the region $0 < \delta < 7$ ms, no synchronization occurred when $\triangle$ was such that $0 < \delta + \triangle < 7$ (that is, initial difference in initial conditions remained), non-synchronous states also occurred for larger $\triangle$. For $\delta > 7$ ms asynchrony was observed for all $\triangle \geq 1$ ms. **B:** Histogram giving the number of occurrences of specific differences, $\triangle$, in spike times of E_1 and E_2 over 20 seconds when $\delta = 20$. Asynchrony manifest as a slow drift to a steady state phase lag. If the initial conditions are close (here $\triangle = 1$ ms), the phase lag takes a long time to appear, order of seconds.

$0 < f' < 1$; hence synchrony will be stable. However, note that a coupling strength of 0.025 is extremely weak when compared to the other currents used in the model.)

This loss of stable synchrony can be understood by considering the effect of the additional distant excitatory synapse on the dynamics of I_h and I_T in a local E-cell. Figure 8B presents the voltage responses of a local excitatory and inhibitory cells as now both receive distant excitatory inputs with delays, δ, between 0 and 7 ms. The solid traces now represent the voltage of the local I-cell, and these traces do not change from those in Fig. 4A. The various dashed traces now represent the voltage of the local E-cell when $\delta = 0$, 4 and 7 ms ($\delta = 0$ ms means no distant input occurred). Immediately after the IPSPs occur in the E-cell with $\delta = 4$ ms and $\delta = 7$ ms, this cell becomes slightly more depolarized than it did for these delays in Fig. 4A. These enhanced depolarizations represent the EPSPs from the additional excitatory to excitatory distant inputs. The size of the EPSP increases as δ

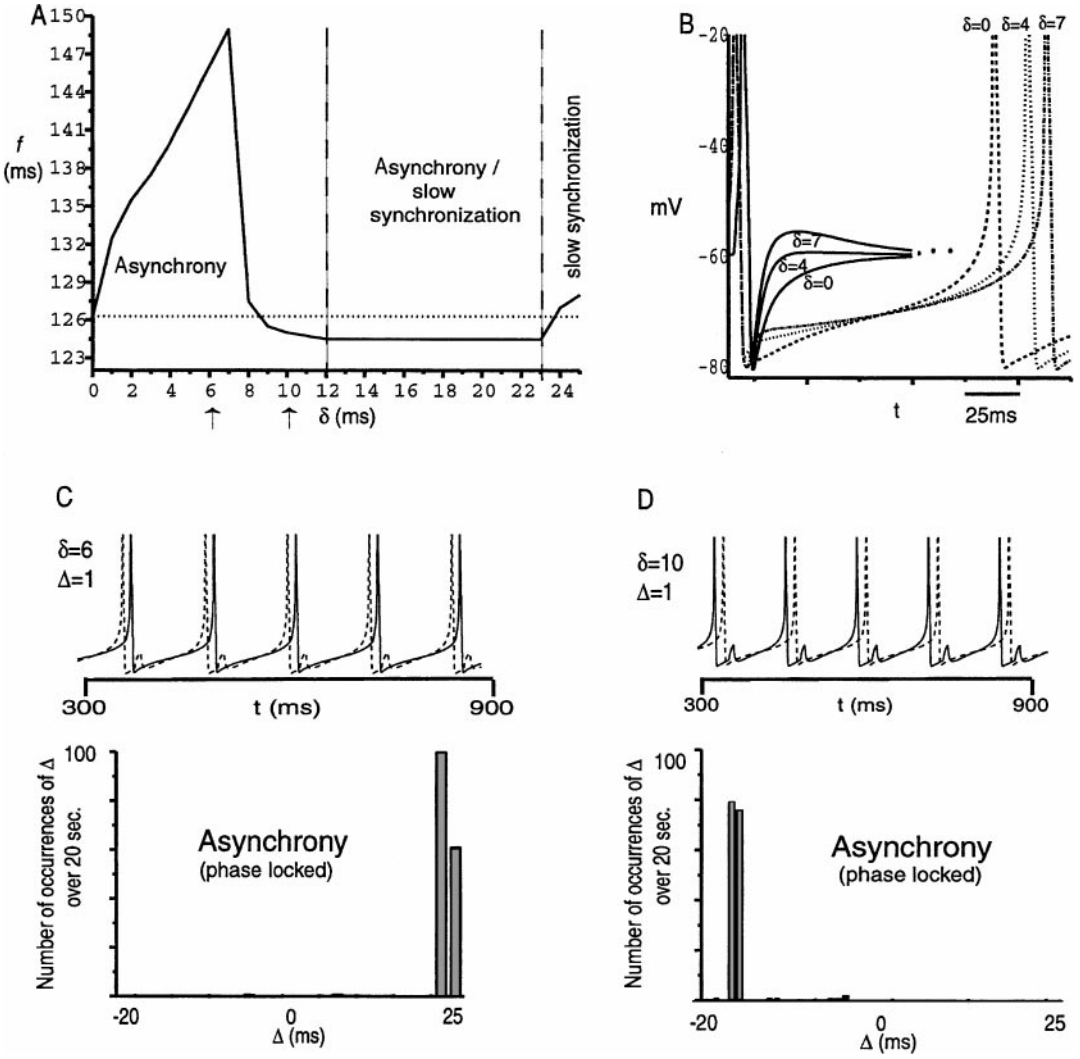

Figure 8. **A:** Graph of f generated with the addition of distant excitatory to excitatory connections (strength 0.05 units) in the network. The dotted horizontal line at ≈ 126 ms represents the period of the excitatory cell without any distant input. Each axis has been cropped; the entire phase of the local circuit (0 to 126 ms or ≈ 8 Hz) is not shown. The graph is separated into three regions. In the region $0 < \delta < 12$ ms, asynchrony occurred for all $\triangle$. For $12 < \delta < 23$ either asynchrony or slow synchronization occurred depending on $\triangle$ and for $\delta > 23$ slow synchronization always occurred. **B:** Voltage versus time cycles of the local excitatory (dashed curves) and local inhibitory (solid curves) cell, which result from distant excitatory inputs arriving to both the excitatory and inhibitory cell at precisely 0 (dashed), 4 (dotted), and 7 ms (dash-dotted) into the local excitatory cell's period. **C and D:** *Top frame:* Voltage traces of E_1 (solid curve) and E_2 (dashed curve) over 600 ms. *Bottom frame:* Corresponding histograms giving the number of occurrences of specific differences, $\triangle$, in spike times of E_1 and E_2 over 20 seconds. **C:** $\triangle = 1$ and $\delta = 6$, **D:** $\triangle = 1$ and $\delta = 10$, in both cases asynchrony manifests as a phase locked steady state.

increases, since as time evolves less inhibition remains to shunt the incoming excitatory current.

As in the network without distant excitatory to excitatory connections, r and h_T begin to slowly increase after the initial hyperpolarization from the inhibitory spike; however, a subsequent EPSP in the excitatory cell decreases the steady state level that each of these variables approaches (see Figs. 5A and 5B). Thus, although the excitatory cell spikes before these variables reach their steady-state values, it takes longer for r and h_T to reach levels that are sufficient to depolarize the cell to a spiking level—that is, it takes longer for sufficient h current activation and T current deinactivation to occur. Hence, the spike time of the excitatory

cell is delayed. These effects intensify as the size of the EPSP increases, resulting in an increase in the slope of f to values bigger than 1 when $\delta < 7$ ms.

We have ignored discussion of m_T, the activation variable of the T current, since its effects are negligible until the T current is sufficiently deinactivated to allow activation of this inward current to be effective. Furthermore, we point out that at increased voltage levels in the excitatory cell (but less than 60 mV) the rate of increase of m_T decreases since $\tau_{m_T}(V)$ gets larger (see Fig. 5E). Thus, as δ increases, the increased EPSPs in the excitatory cell causes m_T to rise slower and this facilitates the delay to spiking (Fig. 8A).

For reasons similar to those given in Section 3.3.1, a region with negative slope begins at $\delta = 7$ ms but now extends to $\delta = 12$ ms. Hence, asynchrony is observed in the network for all $\delta < 12$ ms. Figures 8C and 8D show two representative cases (compare to Fig. 3).

Moreover, in the region $7 < \delta < 12$ ms the maps T_E and T_I discussed in Section 3.3.2 are defined even with distant E to E coupling in the network. The map T_I will be exactly the same and the map T_E will be qualitatively the same. T_I is defined to be the amount of time it takes the local inhibitory cell to spike after it receives distant excitatory input; this time is defined in the region $7 < \delta < 12$ and is independent of E to E coupling. T_E is defined to be the amount of time, after the second inhibitory input is received, for the local E cell to fire; with the weak E to E coupling used in this analysis, the second spike of the local I-cell doublet pair fires before the local E-cell fires again, and hence the same definition of T_E may be used. As in the case without E to E coupling, T_E will increase as δ increases. In both cases, this feature comes from the fact that the second inhibitory spike occurs *earlier* in the period of the local E cell, as δ increases, causing the time between receipt of the second inhibitory input and next fire (that is, T_E) to increase. As in Section 3.3.2, since the map T_I is decreasing and the map T_E is increasing, they will produce a map F_δ that predicts asynchrony in this region.

Finally, for delays $\delta > 12$ ms, f exhibits two regions, and in each of these regions, the network dynamics is qualitatively similar to that observed in the corresponding regions for the original f seen in Fig. 3A. For example, at $\delta = 20$ there is again slow synchronization (data not shown).

3.4.3. Effects of Modulation of Synaptic Coupling Strengths. Synaptic coupling strengths are known to be highly dynamic during various behavior states of an animal (Bressler et al., 1993). In this section we briefly study the effects of modulating the synaptic coupling strengths on the shape of f and on the synchrony of the network.

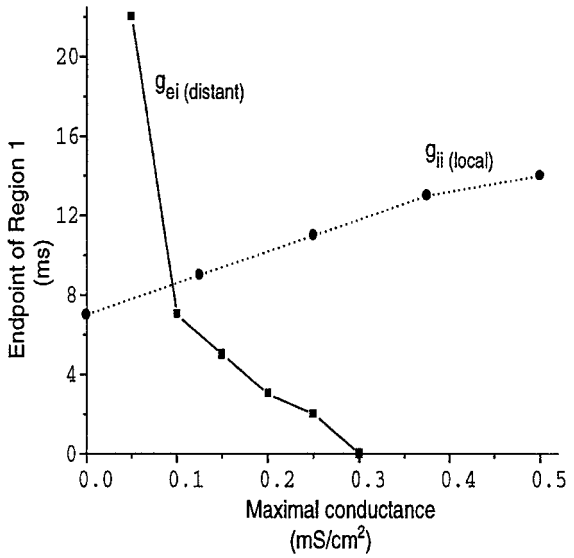

Figure 9. Tracking the endpoint of Region 1 in Fig. 3A as the maximal conductance of the distant excitatory to inhibitory synapse, g_{ei} (solid curve), or the local inhibitory to inhibitory synapse, g_{ii} (dotted curve), is varied. Note: All other parameters are fixed at the values used to generate f in Fig. 3A.

First, as shown by the solid curve in Fig. 9, increasing the maximal conductance level of the distant excitatory to inhibitory synapse, g_{ei} (from its default value 0.1), causes the local inhibitory cell to spike sooner and moves the endpoint of Region 1 in Fig. 3A to the left of $\delta = 7$ ms. By contrast, adding local reciprocal inhibition causes the local inhibitory cell to spike later and moves the endpoint of Region 1 to the right of $\delta = 7$. Moreover, as the maximal conductance strength of this local reciprocal inhibitory coupling, g_{ii}, is increased, the endpoint of Region 1 is moved further to the right (see dotted curve in Fig. 9). Hence, with more local inhibition, neutral synchrony can occur over larger distances.

Finally, adding local reciprocal excitation does not qualitatively affect the shape of f (data not shown).

3.4.4. Effects of Increasing Drive to the Inhibitory Cells. The initial flat portion of the function f ($\delta <$ 7 ms in Fig. 3A) generated from the network configuration in Fig. 1 is significant because it implies that local α-frequency rhythms can be synchronized by common

external input. In particular, the initial phase lag between the E cells is zero when they receive common external input, and since the function f is flat, the phase lag between the E cells remains constant over successive cycles. Moreover, the subsequent negative slope of f implies that networks coupled with delays just beyond the endpoint of this flat region will desynchronize even in the presence of common input. Recall that the initial flat portion of f ends at the first delay in which a second postsynaptic inhibitory spike in the local I-cell (that is, doublet) is produced (see Section 3.3.1); and this delay depends on the excitability of the local inhibitory cell.

In this subsection, we investigate the influence of one factor that controls the excitability of the inhibitory cell—namely, the level of inhibitory-cell drive. We find that when the level of drive to the inhibitory cells is increased the distance over which the network can synchronize via synchronized input is decreased. Note that this was also the case for increased levels of distant excitatory to inhibitory synaptic connection strength, shown above in Section 3.4.3.

The f in Fig. 3A is generated without any constant external drive to the local inhibitory cell. Figure 10 presents f generated with and without the local inhibitory cell receiving a constant level of depolarizing current, I_{app} (dotted curve $I_{\text{app}} = 0.0$, solid curve $I_{\text{app}} = 0.06$, dashed curve $I_{\text{app}} = 0.12$). The dotted horizontal line again represents the intrinsic period of the local excitatory cell without any external drive. Notice that with a small amount of depolarizing current ($I_{\text{app}} = 0.06$) the endpoint of the flat region moves to the left (as compared to the graph with $I_{\text{app}} = 0.0$) and continues to move left as I_{app} increases.

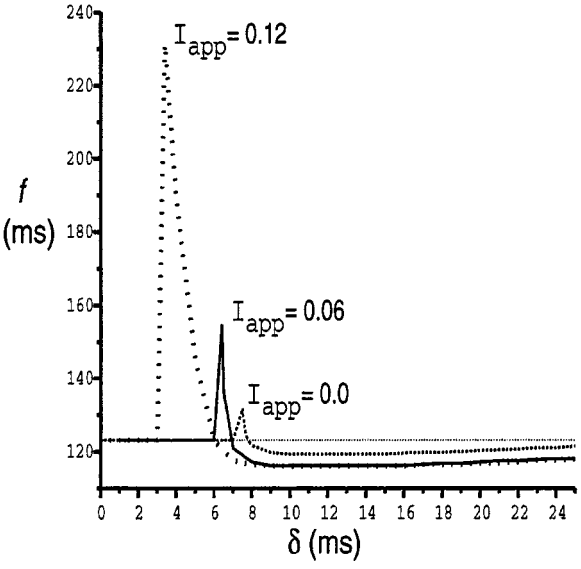

Figure 10. Graph of f generated with a constant depolarizing current applied to the local inhibitory cell, dotted curve $I_{\text{app}} = 0.0$, solid curve $I_{\text{app}} = 0.06$, dashed curve $I_{\text{app}} = 0.12$. The dotted horizontal line at ≈ 126 ms represents the period of the excitatory cell without any distant input.

Beyond the flat portion of f, there is a steep rise in the graph that represents a long delay in the spike time of the excitatory cell. This long delay arises from the fact that at the first δ in which a second inhibitory spike is generated (data points for δ were chosen at 0.1 ms intervals), the inhibitory cell slowly rises to its spiking threshold and thus spikes late in the period of the excitatory cell. The resulting hyperpolarization of the excitatory cell happens late enough in the excitatory cell's period to significantly delay its firing time; and hence, there is a steep rise in f. Although the δ at which a second inhibitory spike occurs decreases as I_{app} increases, the inhibitory cell actually takes longer to spike at this δ as I_{app} increases. Hence, the excitatory cell is delayed longer and there is a *higher* rise in the functions f generated here.

We note that the steep rise in the graph $I_{\text{app}} = 0.0$ is not present in Fig. 3A. For the purposes of Section 3.3, Fig. 3A was generated using intervals of 1 ms between data points for δ as compared to 0.1 ms here.

For both graphs of f in Fig. 10 with I_{app} positive, beyond the region with negative slope, there are two regions qualitatively similar to those of f with $I_{\text{app}} = 0$, a nearly flat region followed by a region with small positive slope. These regions arise from network behaviors analogous to those described in Section 3.3.1.

In conclusion, we have shown that if there is a increase in the level of drive to the inhibitory cells then there is a decrease in the local distance over which α-frequency rhythms can be synchronized. However, the qualitative behavior of long-distance coupled networks will not change.

3.5. A Larger Network

For mathematical simplicity, the analysis in Sections 3.2, 3.3, and 3.4 was based on a minimal network of neurons. In this section, we expand the network model to a larger layer V model that still oscillates in the α-frequency range. The larger model allows us to include potential effects of possible decoupling

within local populations of excitatory and inhibitory cells. We give numerical results verifying that, as predicted, under most conditions asynchrony is observed in the expanded global network.

3.5.1. Expanded Local Model. We expand the local two-cell oscillating unit described in the methods section to a local four-cell unit. This unit consists of two excitatory and two inhibitory cells of the types described in the methods section. Within the local unit, the cells are coupled with all to all synaptic coupling.

The connection strengths of the local synapses are normalized to adjust for the increased number of synapses from and to a cell. Since the number of cells has doubled, the connection strengths of each of the excitatory to inhibitory and the inhibitory to excitatory synapses are half of the strength of those in the local two-cell model. There are excitatory to excitatory AMPA synapses in this four-cell local unit, and we set their connection strengths to be half of the strength of an excitatory to inhibitory synapse. This is done under the assumption that excitatory to excitatory synapses are weaker than excitatory to inhibitory synapses within a localized network (White, 1989). Similarly, inhibitory to inhibitory $GABA_A$ synapses of half the strength of the inhibitory to excitatory synapses are present.

Regardless of initial phase lags, each cell in this four-cell unit oscillates synchronously (with a small delay between the excitatory and inhibitory cells) via rebound spikes as was described in Section 3.1. Using the same parameters for all the intrinsic cellular mechanisms as in the local two-cell model, this local four-cell model sustains rhythmic activity at approximately the same α frequency as the two-cell model.

3.5.2. Global Network Results. To form a larger global network, we connect two of the above described four-cell local network models using both distant excitatory to excitatory and distant excitatory to inhibitory AMPA synapses. We again incorporate a time delay in all synapses between the two local four-cell units to represent spatial distance. We also set all the synaptic connection strengths between units to half of the respective connection strengths within a local four-cell unit. A picture depicting this expanded global network structure can be seen in Fig. 11.

Considering each synchronous local four-cell circuit as a single oscillating unit, the analysis of Section 3.2 holds for this expanded global network. Indeed, numerical simulations of the expanded global network exhibited the same qualitative results as seen for the smaller network and described in Fig. 8A. Figure 12A shows a representative case comparable to Fig. 8D ($\delta = 10$); a minor difference from the smaller network in the manifestation of asynchrony is noted in the figure caption. At $\delta = 20$, as in the smaller network, there is very slow synchronization (after 4 seconds, data not shown). These results are again consistent with the claim that rhythms in the α-frequency range tend not to synchronize over spatially distant areas of the cortex.

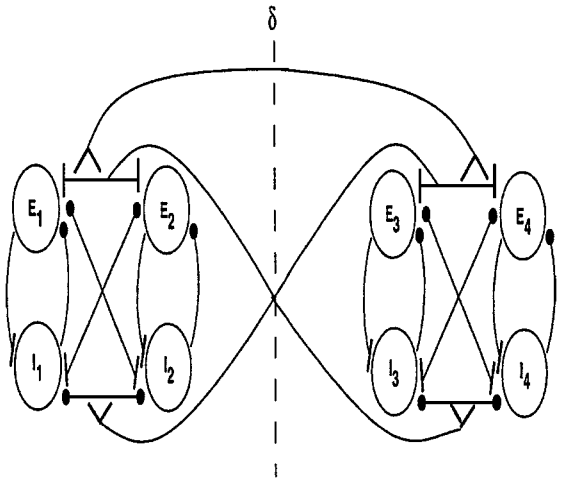

Figure 11. Representation of the expanded global network: two local circuits, each consisting of two excitatory cells with all to all coupling to two inhibitory cells, are connected via long distant excitatory to inhibitory and excitatory to excitatory synapses.

We conjecture that if we continued to increase the number of cells in a network, scaling all the synaptic connection strengths appropriately, the results of this article would hold for arbitrarily large network models.

3.6. Discussion

Motivated by the results of experimental studies, we have constructed a cellular and network-based model for the generation of cortical α-frequency rhythms. The model (without distant excitatory to excitatory synapses) shows that, for locally coupled networks, synchronous α-frequency rhythms induced by initial common initial input can be maintained. The size of the conduction delays over which this holds is influenced by the strength of the distant excitatory to inhibitory synapse as well as the level of constant drive to the inhibitory cell. However, for coupling over most spatial distances, α-frequency rhythms are observed

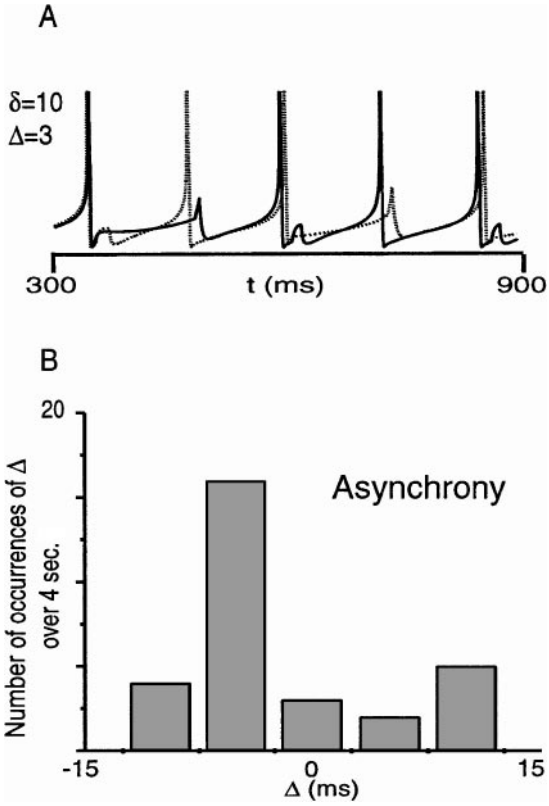

Figure 12. Numerical results of the expanded global network shown in Fig. 11. **A:** Voltage traces of cells E_1 (solid curve—synchronous to E_2) and E_3 (dashed curve—synchronous to E_4) over 600 ms; $\triangle = 3$ and $\delta = 10$. (Note that $\triangle = 3$ represents the initial difference in spike times between E_1 and E_2, E_3 and E_4, and E_1 and E_3.) **B:** Corresponding histograms giving the number of occurrences of specific differences, $\triangle$, in the spike times of E_1 and E_3 over 4 seconds. The network does not reach a steady state. Thus, the figure label states that asynchrony occurs (see also Fig. 8D).

to be asynchronous, and these findings are consistent with recent experimental observations (Roelfsema et al., 1997). We have seen that the same mechanism—namely, the kinetics of I_T and I_h—is responsible for both the generation of the rhythm and its property of asynchrony. Moreover, because I_T and I_h are hyperpolarization-activated inward currents, they essentially invert the roles of excitatory and inhibitory inputs. Hence, our intuitions about the synchronization properties of excitatory to excitatory connections and the role of inhibition in spike timing are reversed. Furthermore, asynchrony is facilitated by the addition of recurrent excitation to the network model and by local inhibition, which decreases the spiking time in excitatory cells. Finally, numerical simulations indicate that the results proven for a minimal representation of a cortical network are robust and also applicable to systems in which the cells of a given type (E or I) are not all lumped together.

3.6.1. Why Does the Reduction to One-Dimensional Maps Work? In order for the one-dimensional maps to work, the general hypotheses of PRC (phase response curve) theory should be at least approximately satisfied. That is, the local oscillators, when perturbed, should return (approximately) to their periodic wave forms within one cycle; also, the effect of the stereotypic perturbation (signal from the other local circuit) should depend only on the time in the cycle of the recipient oscillator that the perturbation is received. The first is true because of the reset properties of the currents, using the fact that the time scale of the oscillation is set by slow activation or deinactivation of the h-and T-currents. Those gating variables are strongly voltage dependent and quickly reset to almost fixed values when the E-cell spikes (see Fig. 5). Though other gating variables, such as activation of the fast spiking K current, do not reset with a spike, their effects are gone by the end of a cycle. This implies that, for these E-I oscillations, the timing of the E-cell spike paces all of the other variables, and there is no history dependence in any of the other variables. If the reset of the "slow" gates is not fast, the behavior of the network can be radically different (LoFaro and Kopell, 1999). Once one has the quick return to the limit cycle, a short (relative to the oscillator period) and stereotypic signal will always lead to a phase shift that is dependent only on the phase at which input is received. In our case, the input signal *is* stereotypic, because it consists of a fixed EPSC delivered to the distant I-cell.

To understand how the above hypotheses constrain the use of this method, we first contrast our current situation with inhibitory coupling in a network of two thalamic interneurons in burst mode (Terman et al., 1996). In that case, the signal between coupled neurons is not short. Instead, the slowly decaying inhibition that forms the coupling signal is on the same time scale as that of the uncoupled oscillator, and the effect of the coupling signal lasts well beyond one cycle. In our case, there is also decaying inhibition, but it is *within* the E-I local circuit itself, while the distant E to I coupling signal between the two local circuits is a fast signal. In Terman et al. (1996), the signal also does not have a stereotypic effect on the postsynaptic cell; there is an interaction between the changing state

of the postsynaptic oscillator and the changing state of the synaptic conductance that varies from cycle to cycle. Hence, PRC methods are not useful. Similarly, in Bose et al. (2000), dealing with two excitatory neurons, there is no reset when the E-cell fires, keeping the history dependence in the gating variable.

Similar reductions have been used for analysis of synchronization of distant pairs of local circuits displaying the gamma and beta rhythms (Ermentrout and Kopell, 1998; Kopell et al., 2000). As in the current article, the signal carrying the information about timing between the circuits is very fast compared to the processes controlling the oscillation (decay of locally produced inhibition for gamma, the latter plus an afterhyperpolarization current for beta). This separation is fundamental to the use of the methods of this article. Other differences in time constants, such as the those of the h-current activation and the T-current activation, are not important in the reduction to a one-dimensional map. However, those separations play an important role in allowing us to understand how the biophysics shapes the one-dimensional map.

3.6.2. Weakly Heterogeneous Global Network. The analysis presented in this article has been for homogeneous global networks. One cannot expect predictions made by the slopes of f to be exact for a network with heterogeneity. However, the results of this analysis can be extended to global networks that have a small amount of heterogeneity.

In particular, α-frequency rhythms will still be asynchronous in regimes where the slope of the graph of f is negative, since small inhomogeneities in the system cannot overcome the desynchronizing effects intrinsic to the model. Similarly, in regimes where the slope is strictly positive, a small amount of heterogeneity in the network would still produce almost synchronous rhythms. However, small amounts of heterogeneity may cause a neutrally stable synchronous solution to become weakly stable or unstable, and in either case there would be long transients.

We tested the above theory by adding a small amount of heterogeneity to the four-cell network depicted in Fig. 1. The heterogeneity was added by simulating injection of a constant depolarizing current into the excitatory and inhibitory cells on one of the two local oscillating units. This resulted in a small increase in frequency (up to 10%) of the depolarized unit. When the local networks were then connected with various conduction delays, δ, and using various differences, $\triangle$, in initial conditions we found that the same qualitative results on the occurrence of synchrony held for all values of δ and $\triangle$ tested as in the case of a homogeneous network. Hence, in the context of the results of this paper, a slightly heterogeneous α-frequency network will tend not to synchronize.

3.6.3. Comparison to Spindle Rhythms. The α-frequency rhythmic activity we have analyzed here, which is thought to be generated in layer V of the cortex during periods of rest or reward, differs in several fundamental respects from the spindling 7 to 12 Hz rhythmic activity observed experimentally in the thalamus and the cortex during the early stages of sleep (Steriade and Deschenes, 1984; Contreras et al., 1998). In this section, we will make a comparison between our model and models generating 7 to 12 Hz spindle oscillations. We first note that thalamic networks do not contain E to E connections; therefore, in this discussion we are making a comparison between thalamic models and our model without E to E connections.

Our model contains several of the same intrinsic and synaptic properties as thalamic network models (Wang et al., 1995; Destexhe and Sejnowski, 1997), but the network behavior is different. In the thalamic models, the I cells (known as RE cells) can generate bursts of activity at α-frequencies via intrinsic T and AHP currents, either as separate cells or as RE networks (Destexhe and Sejnowski, 1997). In our case, the I-cells are nonadapting. The individual E cells in the thalamus, known as TC cells, display bursts of oscillations via the interplay of intrinsic h and T currents; however, these bursts are at lower frequencies between 0.5 and 4 Hz. The RE-TC network generates sustained α-frequency oscillations known as spindles. The individual TC cells do not fire at that frequency but separate into clusters; it is only the population of TC cells that fire at the α-frequency. This differs from our situation in which the E-cells fire on every cycle of the α rhythm.

There are also differences in mechanisms of synchronization or desynchronization. Since there are several kinds of thalamic rhythms, we contrast our mechanisms with synchronization in each of several cases. We start with the network of TC and RE cells in which $GABA_A$ connections are blocked; this removes all RE-RE connections but leaves RE-TC connections via $GABA_B$. Wang et al. (1995) have shown that full synchrony can be obtained due to long bursts of the I cells that come about from lack of intra-RE connections. This synchrony, which is at the much

lower frequency of $\approx$ 4 Hz, is the effect of a common rebound from large simultaneous hyperpolarizations as described by Rubin and Terman (2000). This increase in I-cell drive to the E-cell does not, in our case, produce synchronization. The essential reason is that whether the cells synchronize or not in our case depends on the latency of the I-cell spike from the distant E-cell excitation; changing the strength of the I-cell drive to its local E-cell (the only I-cell drive) does not change the boundaries of the regions of the response function f, or the sign of the slope of f within regions. Therefore, increasing the strength of inhibition to the E-cell cannot change the network from asynchronous to synchronous.

If $GABA_A$ is not blocked, the TC cells do not synchronize, but form clusters (Wang et al., 1995; Destexhe and Sejnowski, 1997). The coherence within the population depends strongly on the divergence of the I to E connections, so that the E-cells within the network get relatively uniform inhibitory inputs. In our case, the E-cells receive inhibition only from their own local I cells, and hence common inhibition plays no role in synchronizing the two separated circuits. Thus, differences in functional connectivity plays a role in differences in synchronization mechanisms.

Finally, the thalamic models above deal with local networks without spatial distribution of the cells; when such spatial distribution is added (in the absence of cortical input (Contreras et al., 1996)), one gets waves, not synchrony (Kim et at., 1995; Destexhe et al., 1996). It remains to be seen if the mechanisms in the current article that produce desynchronization of discrete separated circuits would produce waves in a more continuous medium.

Acknowledgments

We thank G.B. Ermentrout for help with the numerical simulations, K. Josic for contributions in the preliminary stages of this work, and D. Terman for penetrating comments and questions about an earlier draft. N. Kopell received support from NSF grant DMS-9706694 and NIH grant MH47150. S.R. Jones was supported by DMS-9706694. D.J. Pinto was supported by NSF G.I.G. grant DMS-9631755. T.J. Kaper received support from NSF grant DMS-9624471.

References

Bazhenov M, Timofeev I, Steriade M, Sejnowski TJ (1998) Cellular and network models for intrathalamic augmenting responses during 10 Hz stimulation. *J. Neurophysiol.* 79:2730–2748.

Bose A, Kopell N, Terman D (2000) Almost-synchronous solutions for mutually coupled excitatory neurons. *Physica D* 140:69–94.

Bressler SL, Coppola R, Nakamura R(1993) Episodic multiregional cortical coherence at multiple frequencies during visual task performance. *Nature* 366:153–156.

Castro-Alamancos MA, Connors BW (1996) Cellular mechanisms of the augmenting response: Short-term plasticity in a thalamocotrical pathway. *J. Neurosci.* 16(23):7742–7756.

Castro-Alamancos MA, Connors BW (1996) Short-term plasticity of a thalamacortical pathway dynamically modulated by behavioral state. *Science*, reprint series, 272:274–277.

Connors BW, Amitai Y (1997) Making waves in the neocortex. *Neuron* 18:347–349.

Contreras D, Destexhe A, Sejnowski TJ, Steriade M (1996) Control of spatiotemporal coherence of a thalamic oscillation by corticothalamic feedback. *Science* 274:771–774.

Contreras D, Destexhe A, Sejnowski TJ, Steriade M (1998) Spatiotemporal patterns of spindle oscillations in cortex and thalamus. *J. Neurosci.* 17(3):1179–1196.

Crook SM, Ermentrout GB, Bower JM (1998) Spike frequency adaptation affects the synchronization properties of networks of cortical oscillators. *Neural. Comput.* 10:837–854.

da Silva, LF (1991) Neural mechanisms underlying brain waves: From neural membranes to networks. *Electroenceph. Clin. Neurophysiol.* 79:81–93.

Destexhe A, Babloyantz A, Sejnowski TJ (1993) Ionic mechanisms for intrinsic slow oscillations in thalamic relay neurons. *Biophys. J.* 65:1538–1552.

Destexhe A, Bal T, McCormick DA, Sejnowski TJ (1996) Ionic mechanisms underlying synchronized oscillations and propagating waves in a model of ferret thalamic slices. *J. Neurophysiol.* 76(3):2049–2070.

Destexhe A, Mainen ZF, Sejnowski TJ (1998) Kinetic models of synaptic transmission. In Koch C, Segev I, eds., *Methods in Neuronal Modeling* (2nd ed.). MIT Press, Cambridge, MA.

Destexhe A, Sejnowski TJ (1997) Synchronized oscillations in thalamic networks: Insights from modeling studies. In: Steriade M, Jones EG, McCormick DA, eds., *Thalamus: Organization and Function*, vol. 1. Elsevier, Oxford.

Devaney RL (1992) *A First Course in Chaotic Dynamical Systems: Theory and Experiment*. Addison-Wesley, Reading, MA.

Ermentrout GB, Kopell N (1998) Fine structure of neural spiking and synchronization in the presence of conduction delays. *Proc. Natl. Acad. Sci. U.S.A. Neurobiology* 95:1259–1264.

Farmer SF (1998) Rhythmicity, synchronization and binding in human and primate motor systems. *J. Physiol.* 509.1:3–14.

Flint AC, Connors BW (1996) Two types of network oscillations in neocortex mediated by distinct glutamate receptor subtypes and neuronal populations. *J. Neurophysiol.* 75(2):951–956.

Fries P, Roelfsema PR, Engel AK, König P, Singer W (1997) Synchronization of oscillatory responses in visual cortex correlates with perception in interocular rivalry. *Proc. Natl. Acad. Sci. U.S.A. Neurobiol.* 94:12699–12704.

Golomb D, Amitai Y (1997) Propagating neuronal discharges in neocortical slices: Computational and experimental study. *J. Neurophysiol.* 78:1199–1211.

Hansel D, Mato G, Meunier G (1995) Synchrony in excitatory neural networks. *Neural Comput.* 7:307–337.

Hirsh JA, Gilbert CD (1991) Synaptic physiology of horizontal connections in the cat's visual cortex. *J. Neurosci.* 11(6):1800–1809.

Huguenard JR, McCormick DA (1992) Simulation of the currents involved in rhythmic oscillations in thalamic relay neurons. *J. Neurophysiol.* 68(4):1373–1383.

Karbowski J, Kopell N (2000) Multispikes and synchronization in a large-scale neural network with delays. *Neural Comp.* 12:1576–1606.

Kim U, Bal T, McCormick DA (1995) Spindle waves are propagating synchronized oscillations in the ferret LGNd in vitro. *J. Neurophysiol.* 74:1301–1323.

König P, Engel AK, Singer W (1995) Relation between oscillatory activity and long-range synchronization in cat visual cortex. *Proc. Natl. Acad. Sci. U.S.A., Neurobio*. 92:290–294.

Kopell N, Ermentrout GB, Whittington M, Traub RD (2000) Beta rhythms have different synchronization properties than gamma rhythms. *Proc. Natl. Acad. Sci. USA* 97:1867–1872.

Kristiansen K, Courtois G (1949) Rhythmic electrical activity from isolated cerebral cortex. *EEG Clin. Neurophysiol.* 1:265–272.

LoFaro T, Kopell N (1999) Timing regulation in a network reduced from voltage-gated equations to a one-dimensional map. *J. Math. Biol*. 38:479–533.

Mainen ZF, Joerges J, Huguenard JR, Sejnowski TJ (1995) A model of spike initiation in neocortical pyramidal neurons. *Neuron* 15:1427–1439.

McCormick DA, Huguenard JR (1992) A model of the electrophysiological properties of thalamocortical relay neurons. *J. Neurophysiol.* 68(4):1384–1400.

McCormick DA, Pape HC (1990b) Properties of a hyperpolarization-activated cation current and its role in rhythmic oscillation in thalamic relay neurons. *J. Physiol.* 431:291–318.

McCormick DA, Pape HC (1990a) Noradrenergic and serotonergic modulation of a hyperpolarization-activation cation current in thalamic relay neurons. *J. Physiol.* 431:319–342.

Pinsky PF, Rinzel J (1994). Intrinsic and network rhythmogenesis in a reduced Traub model for CA3 neurons. *J. Comput. Neuro.* 1:39–60.

Roelfsema P, Engel AK, König P, Singer W (1997) Visuomotor integration is associated with zero time-lag synchronization among cortical areas. *Nature* 385:157–161.

Rubin JE, Terman D (2000) Geometric analysis of population rhythms in synaptically coupled neuronal networks. *Neural Comput.* 12(3):597–648.

Silva LR, Amitai Y, Connors BW (1991) Intrinsic oscillations of neocortex generated by layer 5 pyramidal neurons. *Science* 251:432–435.

Steriade M, Deschenes M (1984) The thalamus as a neuronal oscillator. *Brain Res. Rev.* 8:1–63.

Terman D, Bose A, Kopell N (1996) Functional reorganization in thalamocortical networks: Transition between spindling and delta sleep rhythms. *Proc. Natl. Acad. Sci. USA* 93:15417–15422.

Traub RD, Whittington MA, Buhl EH, Jefferys JGR, Faulkner HJ (1999) On the mechanism of the γ-β frequency shift in neuronal oscillations induced in rat hippocampal slices by tetanic stimulation. *J. Neurosci.* 19:1088–1105.

Traub RD, Whittington MA, Stanford IM, Jefferys JGR (1996) A mechanism for generation of long-range synchronous fast oscillations in the cortex. *Nature* 383:621–624.

Van Vreeswijk C, Abbott LF, Ermentrout GB (1994) When inhibition not excitation synchronizes neural firing. *J. Comp. Neurosci.* 1:313–321.

von Stein A, Chiang C, König P (1999) The role of alpha and gamma frequency interactions in top-down processing in the cat. *Soc. Neurosci. Abstr.* 24.

von Stein A, Rappelsberger P, Sarnthein J, Petsche H (1999) Synchronization between temporal and parietal cortex during multimodal object processing in man. *Cerebral Cortex* 9:137–150.

Wang XJ, Golomb D, Rinzel J (1995) Emergent spindle oscillations and intermittent burst firing in a thalamic model: Specific neuronal mechanisms. *Proc. Natl. Acad. Sci. USA* 92:5577–5581.

White EL (1989) *Cortical Circuits: Synaptic Organization of the Cerebral Cortex*. Birkhäuser Boston, Boston.

Wong RK, Traub RD, Miles R (1986) Cellular basis of neuronal synchrony in epilepsy. *Adv. Neurol.* 44:583–593.